Excited state absorption and relaxation dynamics in a series of heptamethine dyes under femtosecond and nanosecond excitations

Excited State Absorption and Relaxation Dynamics in a series of Heptamethine Dyes for Femtosecond and Nanosecond Excitations

Krishnandu Makhal[1], Sidharth Maurya[2], and Debabrata Goswami*[1,2]

[1]Department of Chemistry, Indian Institute of Technology Kanpur, Kanpur, Uttar Pradesh, Pin-208016, India
[2]Center for Lasers and Photonics, Indian Institute of Technology Kanpur, Kanpur, Uttar Pradesh, Pin-208016, India

*E-mail: dgoswami@iitk.ac.in

Abstract
We show that the near-infrared-absorbing polymethine cyanine dyes exhibit nonlinear absorption (NLA) in the visible region, where they have negligible or no linear absorption. In chloroform solvent, the studied cyanines were found to be photo-unstable and exhibited photo-degradation under prolonged exposures as compared to methanol and dimethylsulphoxide solvents, where they were stable. Excitation with femtosecond (fs) pulses in the visible region (400 nm – 750 nm) exhibits excited state absorption (ESA) as characterized by positive differential absorption (ΔOD) in transient absorption signal. Non-resonant excitations in the visible region are governed by reverse saturable absorption (RSA) mechanism leading to ESA. Excitation with nanosecond pulses also shows NLA owing to ESA from triplet states as compared to that from singlet states under fs excitations. Single beam Z-scan studies were performed with nanosecond (ns) pulses to evaluate ground (σ_{gr}) and excited state (σ_{ex}) absorption cross-sections, which confirms the mechanism of RSA as σ_{ex} were found to be greater than σ_{gr}. The population relaxation from higher excited singlet states shows ultrafast behavior with multi-exponential decay components. The fast time component decay varies from a few hundreds of fs (τ_1) to some hundreds of picoseconds (τ_2), and the long-time decay is in the ns domain (τ_3).

1. Introduction

Polymethine or cyanine dyes are molecules containing polymethine bridges between two nitrogen atoms characterized by the presence of two heterocyclic moieties. These moieties act as both electron donors and acceptors and are connected by a single or an odd number of methine groups in which (n+1) π-electrons are distributed over n atoms [1] producing a delocalized cation across the methine chain [2]. Because of their extended delocalized π-conjugation, they have found multiple applications in optical storage and processing [3], imaging of biological samples [4-6], light-energy conversion [7,8], nonlinear optics [9], optical limiting [10], sensitization [11], etc. The electronic structures of cyanine dyes are usually determined by an odd number of conjugated p_z orbitals and an even number of π electrons associated with them [12,13]. The resulting nodal structure of the π and π* orbitals in these dyes makes the first excited singlet state to be significantly stabilized in comparison to the S_2 state [14]. The absorption spectra of cyanine dyes comprised of an intense $S_0 \rightarrow S_1$ transition in the visible or near-IR region, and $S_0 \rightarrow S_n$ ($n \geq 2$) transitions of much less intensity in the near-UV region [15]. Since the (S_2 - S_1) energy gap ($\Delta E_{S2\text{-}S1}$) in some cyanines are ~1 eV, the coupling between these states are significantly reduced in comparison to typical chromophores [16]. In addition to energy bindings, due to their larger size, structural inertia in these dyes reinforce the slow structural relaxation, which infers that the energy surface of the upper excited singlet states is reconnoitered slowly after excitation [17]. The slow $S_2 \rightarrow S_1$ internal conversion observed in many cyanine dyes [18-20] can be explained by the above-mentioned features.

Several theoretical approaches were also developed in addition to the experimental investigations for understanding the nature of the electronic transitions in polymethine dyes (PDs). The first in this attempt was the Huckel molecular orbital method and the Kuhn free- electron or "metallic model," which were modified to explain the dark color of PDs containing an extended chain of methane groups as the main component [21-24]. These theories were based on the alternation of the charge density along the chain, as proposed by Konig [25]. In 1966 all existing methodologies were incorporated by Dahne [26-29] into a single theoretical concept known as the triad principle. According to this principle, all conjugated organic molecules can be characterized by three ideal states: the aromatic, the polyene and the polymethine state. Based on triad theory, there are two characteristic properties of PDs: the first one equals the single and double bond lengths, and the second one is the definitive alteration of the positive and negative charges at the carbon atoms [30]. In spite of the C-C bond lengths remaining practically unchanged, a substantial change of the atomic charges occurs as a result of excitation. These structural features of the cyanine dyes account for the high $S_0 \rightarrow S_1$ electronic transition, which is accompanied by a considerable p-electron density transfer from the carbon atoms in odd positions to the ones in the even locations. Thus, a maximum $S_0 \rightarrow S_1$ transition probability combined with relatively low transition energy is a characteristic feature of the PDs. The absorption and fluorescence bands of polymethines can be shifted from the visible to the IR-region by increasing the polymethine chain length or by introducing specific terminal groups possessing large p-electron systems [31]. Dyes and organic chromophores with the long-lasting upper excited state have important applications since the energy available through the population of the higher singlet state can be ominously larger than that of the S_1 state (~3 eV for the S_2 state in certain cyanines as compared to $1.5 - 2$ eV for the S_1 state). The long S_2 lifetime in certain cyanines found applications in optical limiting [20,32,33].

In this context, polymethine dyes have strong absorption that is selective to the near-infrared region and span over a broad spectral range. The structural modification allows a shift of their absorption bands to the near-infrared (NIR) region, thereby expanding the existing areas of applications, and exposes new ones, such as highly efficient nonlinear optical materials for all-optical signal processing [34]. Recently, few works have been reported that address the excited state absorption (ESA) properties of cyanine dyes in the visible and IR wavelengths [35-38]. None of the molecules examined here, to the best of our knowledge, has ever been used for nonlinear studies in the visible region nor has ever been studied at a non-resonant excitation wavelength of 400 nm with femtosecond resolutions. We analyze the ESA spectra and the lifetime dynamics of five new heptamethine dyes namely IR-783, IR-792, IR-797, IR-806 and IR-820 which absorbs in the wavelength range from 780 nm to 820 nm, respectively. Upon 400 nm femtosecond excitations, we observe the ESA band (450 nm to 650 nm) in these molecules that appear to the blue of the $S_0 \rightarrow S_1$ (780 to 820 nm) absorption band, which is correlated to the ESA mediated reverse saturable absorption (RSA) that, in turn, is attributed to the $S_1 \rightarrow S_n$ transient absorption. Probing within this ESA band, e.g., at 527 nm but with nanosecond pulses, we still detect the expected ESA. However, the observed ESA corresponds to $T_1 \rightarrow T_n$ absorption rather than from $S_1 \rightarrow S_n$ absorption as in the case of femtosecond or picosecond excitations. Since pulses of 100 ns pulse

widths facilitate the population transfer to the first triplet state from excited singlet states via intersystem crossing (ISC), changing laser pulse widths at a fixed wavelength eventually results in the population transfer to the triplet states. The absorption cross-sections and nonlinear refractive indices obtained from Z-scan studies indicate that these dyes can also act as potential materials in the visible regions (within the ESA band) for optical limiting purposes. These dyes already have numerous existing uses in the near IR region, e.g., in the field of photosensitizers, in photography and photodynamic theory, fluorescent probes in chemistry and biology, materials for electroluminescence and so on. The motivation for the current investigation arises from the fact that these cyanines have never been explored in the visible region as compared to their vast exploration in the near infra-red region. Our recent study thus illustrates the importance of these chromophores in the visible regime as a consequence of novel nonlinear absorption mechanism thereby enabling wider applicability in the visible region of the electromagnetic spectrum.

2. Materials and Experimentation

All the cyanines under study were obtained from Sigma Aldrich and were used as received. Sample solutions were prepared in HPLC grade methanol (MeOH), Chloroform ($CHCl_3$) and dimethyl sulphoxide (DMSO) solvents (Merck, India) at 0.1 mM concentration in 1 mm path length quartz cuvette (Hellma) for experiments. The molecular structure of the heptamethine dyes and their linear absorption spectrum in the studied solvents are shown in Fig. 1 and Fig. 2 respectively.

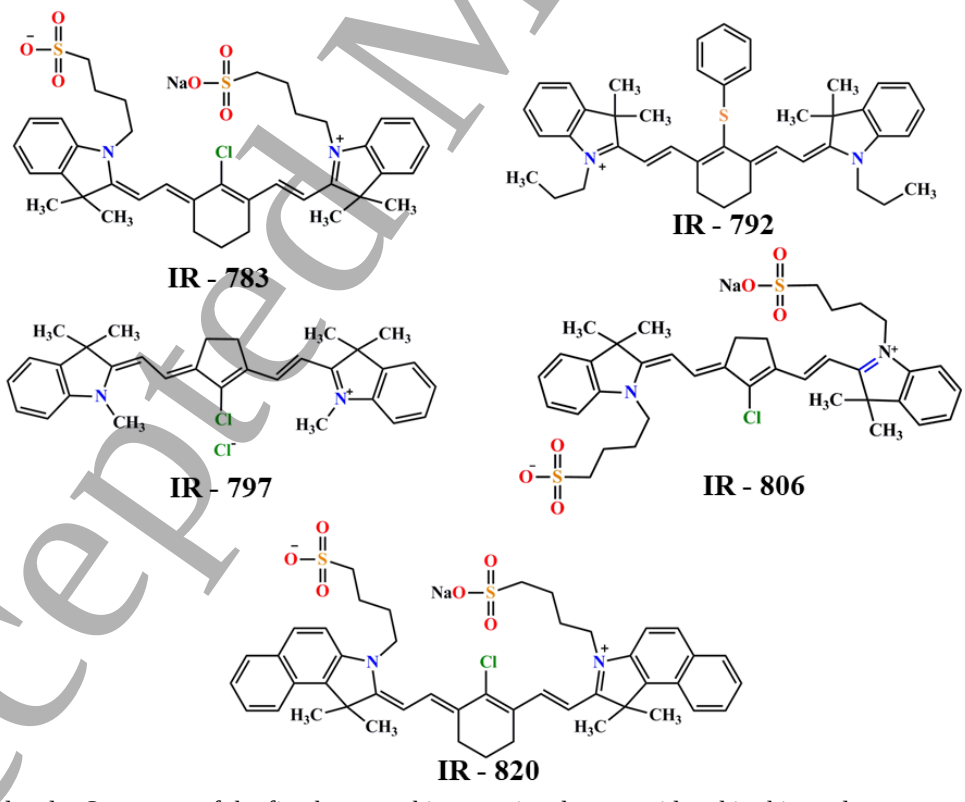

Figure 1. Molecular Structures of the five heptamethine cyanine dyes considered in this study

For femtosecond studies, a mode-locked Ti:Sapphire femtosecond oscillator and a Ti:Sapphire amplifier (Spitfire Pro XP, Spectra-Physics) pumped by a 20-W Q-switched Nd:YLF laser (Empower, Spectra-Physics) was employed. The output from the amplifier generates 50-fs pulses, centered at 800 nm, with a 1-kHz repetition rate and of ~4 mJ energy per pulse. Femtosecond transient absorption measurements were performed in a commercially available spectrometer (Femto-Frame-II, IB Photonics). The beam from the amplifier output was split into two using a beam splitter with the significant part being used to generate the pump pulses. Frequency doubling was done through a β-barium borate (BBO) crystal. A small portion of the original light was allowed to pass through a computer-controlled motorized delay stage and was used to generate a white-light continuum with a spectral range of 450−750 nm by focusing it onto a sapphire crystal. All measurements were performed with pump energy of ~1 μJ, with pump polarization set at a magic angle (54.7°) vis-à-vis the probe beam. The probe was delayed in time w.r.t to the pump pulse with the help of optical delay line providing a maximum delay of 2.0 ns. The probe beam after passing through the sample cell was focused onto a 200-μm fiber optic cable which was dispersed using a polychromator into a CCD camera.

For Z-scan studies, a frequency doubled Q-switched Nd:YVO_4 laser (Evolution 15, Coherent Inc.) was used as nanosecond laser source operating at 250 Hz with a central wavelength at 527 nm with perfect Gaussian shaped 100 ns pulses. A 25 cm lens was used to focus the beam into the quartz cuvette containing sample solutions mounted on a stepper motor driven stage of resolution 0.1 μm and controlled by LabVIEW software interfaced with GPIB through a GHz fast oscilloscope linked to a PC. In our experimental setup simultaneous transmittance measurements of both open aperture (OA) & close aperture (CA) experiments were performed where the output of the laser beam after passing through the sample was collected with the help of two silicon biased fast photodiode (DET 10A Thorlabs) and for collecting reference the third photodiode of same make & model was used.

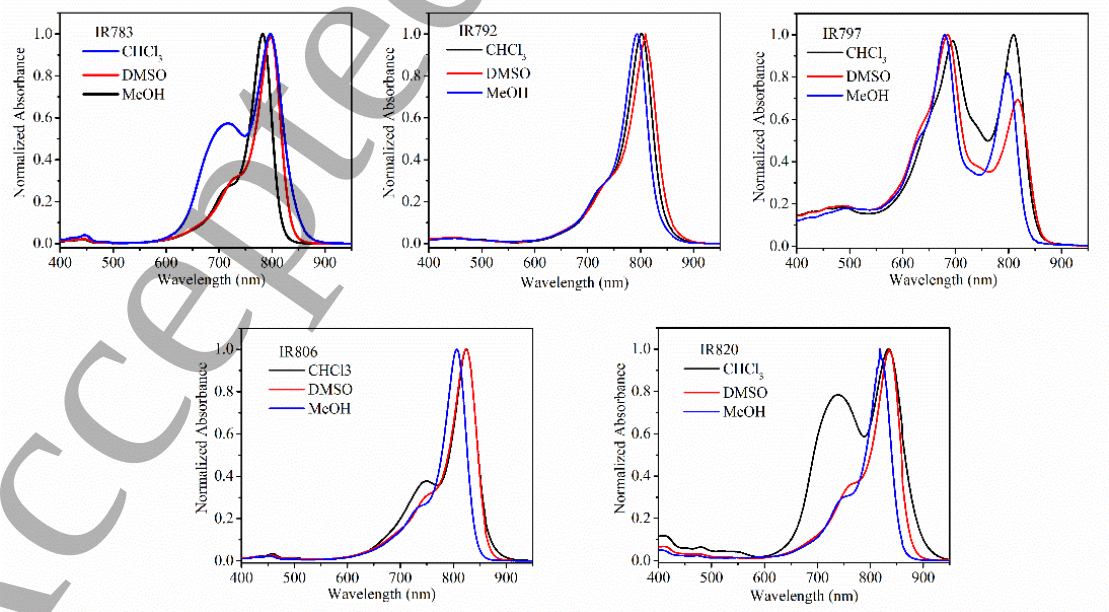

Figure 2 Normalized Absorption spectra of the studied heptamethine dyes in solvents mentioned in the inset

For 527 nm nanosecond pulses, intensities in the range of (3-32) MW/cm^2 at the focus (I_0) were used. Beam parameters used for the experiment were ~40 μm corresponding to Rayleigh range of 9.5 mm. Therefore in the present study, the sample thickness (1mm) is less than the Rayleigh range which satisfies thin cell approximation [39]. The experimental setup was standardized with Rhodamine-B dye, and the whole set of experiments were performed at 295 K. The absorption spectra of the five dyes in three solvents namely MeOH, $CHCl_3$ and DMSO are shown in figure 2.

3. Results and Discussions

All the five chosen heptamethine molecules are near infrared absorbing and have linear absorption maxima positioned between 780-820 nm in the three solvents as represented in figure 2. The effects of solvent on absorption spectra provides important information about solute-solvent interactions, and among the three solvents chosen, all the molecules were photostable in MeOH and DMSO but were unstable, exhibited degradation and were prone to aggregation in $CHCl_3$ under prolonged exposures. We have purposefully chosen these three solvents as these dye molecules exhibit excellent solubility at normal conditions and we want to depict the influence of these solvents on the photostability of the molecules and to predict their nonlinear behavior at non-resonant visible excitations. Concerning the recorded absorption spectra, we found that all the five dyes have the singlet ($S_0 \rightarrow S_1$) absorption in the wavelength range 780-810 nm with an additional absorption band arising in case of $CHCl_3$ solvent at 690-710 nm for IR-783, IR-797, and IR-820 respectively. These features indicate that the three dyes interact differently with the $CHCl_3$ solvent due to the different solute-solvent interactions. The molar extinction coefficients were found to be ~(257000 & 250000) $M^{-1} cm^{-1}$ for IR-783, ~(165000 & 158000) $M^{-1} cm^{-1}$ for IR-797, ~(255000 & 251000) $M^{-1} cm^{-1}$ for IR-792, ~(279000 & 270000) $M^{-1} cm^{-1}$ for IR-806 and finally ~(250000 & 20000) $M^{-1} cm^{-1}$ for IR-820 at their corresponding absorption maxima in MeOH and DMSO solvents respectively. However, it was found that the extinction coefficients for the five heptamethine dyes in $CHCl_3$ were drastically lowered compared to MeOH and DMSO solvents at their respective absorption maxima. The extinction coefficients were found to be ~199000 $M^{-1} cm^{-1}$ for IR783, ~180000 $M^{-1} cm^{-1}$ for IR-792, ~103000 $M^{-1} cm^{-1}$ for IR-797, 203000 $M^{-1} cm^{-1}$ for IR-806 and finally 130000 $M^{-1} cm^{-1}$ for IR-820 respectively with an estimated error of less than ±5%. Another important feature to note is the bathochromic shift of the absorption maxima for each of the dye molecules when the solvent was varied from MeOH to DMSO till $CHCl_3$. The solvent polarity decreases as MeOH>DMSO>$CHCl_3$, and the maximum red-shift in the absorption wavelength is observed for $CHCl_3$, which confirms that these molecules are solvatochromic. In other words, the blue (hypsochromic) shift in absorption maxima with increasing solvent polarity is observed for all the five heptamethine dyes, which essentially reflects negative solvatochromism. Negative solvatochromism in the five cyanine dyes results from the differential solvation of the highly dipolar, zwitterionic electronic ground state and less dipolar first excited state. Methanol and dimethylsulphoxide are polar solvents, and since all the molecules are also dipolar, thus the forces responsible for the hypsochromic shift are dipole-dipole forces and not the dipole-induced dipole forces as in the case if nonpolar chloroform

solvent. This behavior is established in the proceeding sections where we show that different measurable physical properties arise resulting in entirely different chemical dynamics when the solvent is varied. These observations confirm that photo-instability is maximum in the $CHCl_3$ solvent.

The variation observed in case of $CHCl_3$ solvent is a result of intermolecular solute-solvent interaction forces only (which includes effects from ion-dipole, dipole-dipole, and hydrogen bonding interactions), which tend to alter the energy difference between ground and excited state of the absorbing cyanines. Thus we expect different absorption cross-sections of ground and excited states leading to the observation of new photophysical phenomena. The spectral variations which arise from modification of the chemical nature of the dyes by the solvent medium, such as solvent-dependent aggregation, ionization, and complexation were not the causes of concern in our case. We used very low dye concentrations and low average power far below their ionization regime for our experiments which eliminates the possibility of ionization and aggregation under current investigation. The possibility of complexation could also be ruled out because of the absence of chelating groups in the molecule and absence of dual absorbance bands in the absorption spectrum in the solvents studied.

Two different sets of experiments were conducted in the visible region to test the response of these molecules in the above solvents. First one was the investigation of nonlinear absorption and refraction at 527 nm which is non-resonant for linear absorption and has negligible absorption at and near this wavelength region. The pulse width of 100 ns at 250 Hz was utilized to carry out open and closed aperture experiments. The experimental data obtained under this study are shown in figure 3. The outcome and fit of the experimental data are presented according to solvents, MeOH first, followed by DMSO and finally in $CHCl_3$. Among the dye solutions used those prepared in MeOH and DMSO solvents were photo-stable and remained un-degraded even after the experiment. While in the $CHCl_3$ majority of the dye underwent chemical changes and photo-degradation upon excitation. Among the five heptamethine dyes, all, but IR-797 and IR-820, were less stable as compared to the other three and degraded at very low average powers suggesting that the power threshold for these dyes are very low and are not suitable for nonlinear studies in the visible region at high average laser powers.

Nevertheless, we have performed the experiments and extracted the nonlinear absorption and refraction coefficients at very low average powers with careful experimentation and analysis. We found that even at low average laser powers and at non-resonant excitations in the visible region we can detect the nonlinear absorption and refraction owing to ESA. The mechanism of ESA resulting from reverse saturable absorption (RSA) operates at visible wavelength excitations. The RSA behavior is the result of absorption from higher singlet or triplet excited states to upper excited states resulting in the decrease of transmitted light intensity as seen as a dip in the open aperture Z-scan traces. The RSA is further supported by the plot of β (nonlinear absorption coefficient) versus I_0 (Intensity at the focus) as shown in Fig. 4 for all the molecules at different input intensities.

A steady increase or decrease in the plot of β versus I_0 is proof of the RSA process [40,41]. Nonlinear absorption and refraction coefficients were extracted from the fit to experimental data as per the theoretical expression given by [42,43]:

$$T(z) = 1 - {}^{q_0}/_{2\sqrt{2}} \qquad \text{for} \quad |q_0|<1 \tag{1}$$

T(z) is the transmittance at various z positions, and the free factor q_0 is defined as

$$q_0 = \frac{\beta I_0 (1 - e^{-\alpha_0 L})}{(1 + \frac{z^2}{z_0^2})\alpha_0} = \frac{\beta I_0 L_{eff}}{(1 + \frac{z^2}{z_0^2})}$$

where α_0 is the linear absorption coefficient, L is the thickness of the sample, I_0 is the intensity at the focus (z=0), and z_0 is the Rayleigh range. Equation 1 is used for the calculation of β from open aperture traces. Excited-state and ground-state absorption cross-sections were calculated from the relation [39,44]:

$$T = \frac{\ln\left(1 + \frac{q_0}{1+x^2}\right)}{\left(\frac{q_0}{1+x^2}\right)} \tag{2}$$

where $x=z/z_0$ and z_0 is the Rayleigh range, while z is the distance of the sample from the focus. q_0 is given by

$$\boldsymbol{q_0 = \frac{\sigma_{ex}\alpha_0 F_0 L_{eff}}{2h\nu}}$$

from which σ_{ex} is calculated. Where F_0 is the on-axis fluence at the focus which is related to incident input energy over the sample. Finally, the ground state absorption cross-section σ_{gr} is calculated using the relation:

$$\sigma_{gr} = {}^{\alpha_0}/_{N_A C} \tag{3}$$

The values were obtained from a theoretical fit to experimental data as shown in figure 3. In cases where no open aperture plots were obtained, the nonlinear absorption coefficient "β" is evaluated from the corresponding close-aperture trace of that compound, which is because the closed-aperture Z-scan trace alone can provide both β and γ values (nonlinear index of refraction) [45,46]. As evident from these results, it can thus be concluded that these near-IR absorbing dyes act as efficient nonlinear absorbers in the visible region in MeOH and DMSO solvents and can, therefore, be used as potential future materials for optical limiting and other nonlinear applications.

However, we could not obtain good quality data for open aperture (OA) cases for some of the molecules in certain solvents under the exact and similar experimental conditions where all the other molecules exhibited nonlinear absorption and refraction. These include OA for IR820 in MeOH, IR797 in DMSO,

IR820 in DMSO, IR797 and IR820 in $CHCl_3$ respectively. Therefore the OA Z-scan plots are not shown here for the molecules above.

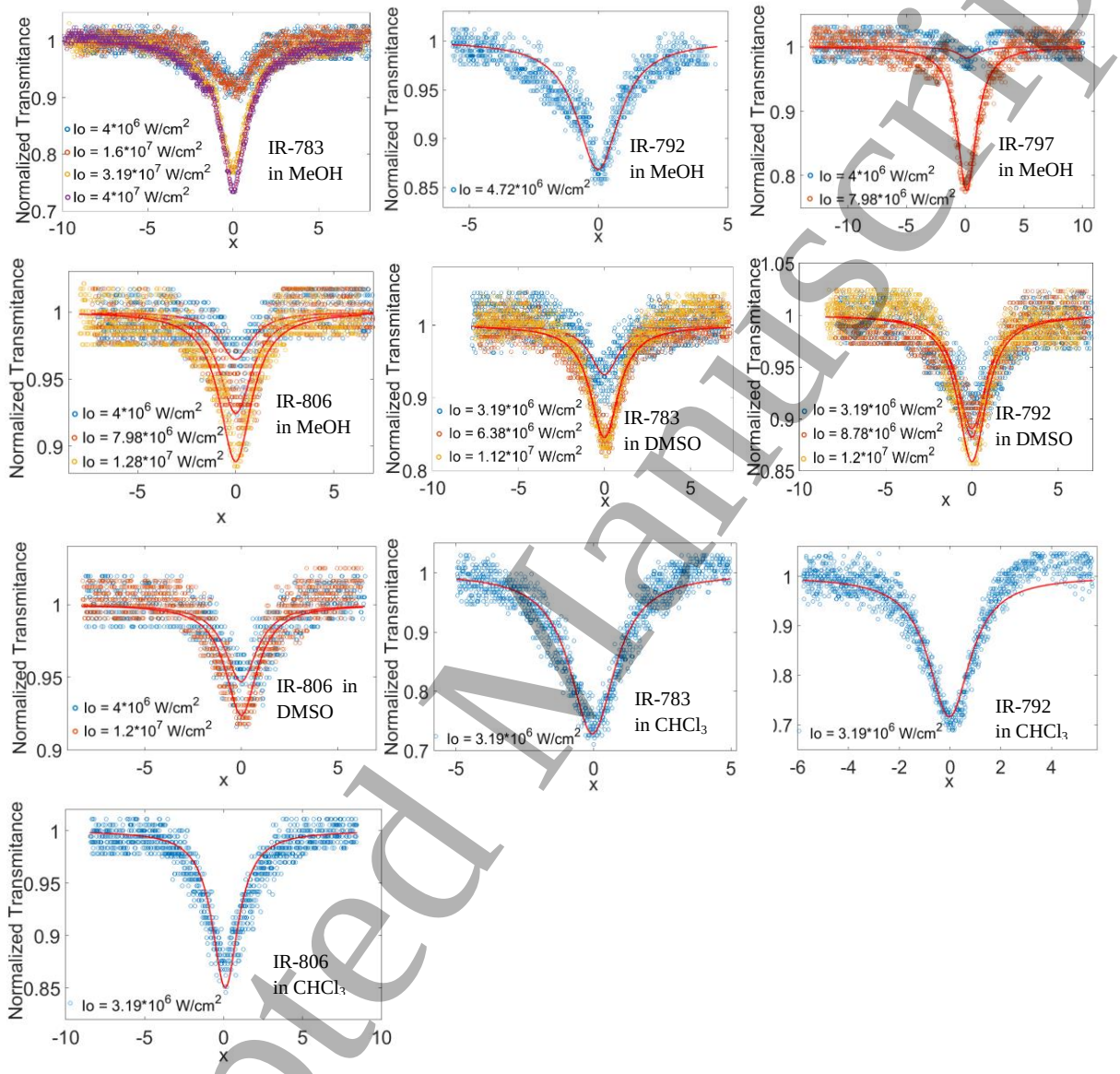

Figure 3 (a). Open Aperture traces of the heptamethine dyes representing characteristic nonlinear absorption at far off from their corresponding resonant absorption. Intensities at which the data were taken in the solvents used are mentioned in the respective insets. Where $x=z/z_0$ (z_0 is Rayleigh range, and z being distance scanned from one end to other via focus). Raw data points are represented in circles, and theoretical fits are represented in solid colored red lines.

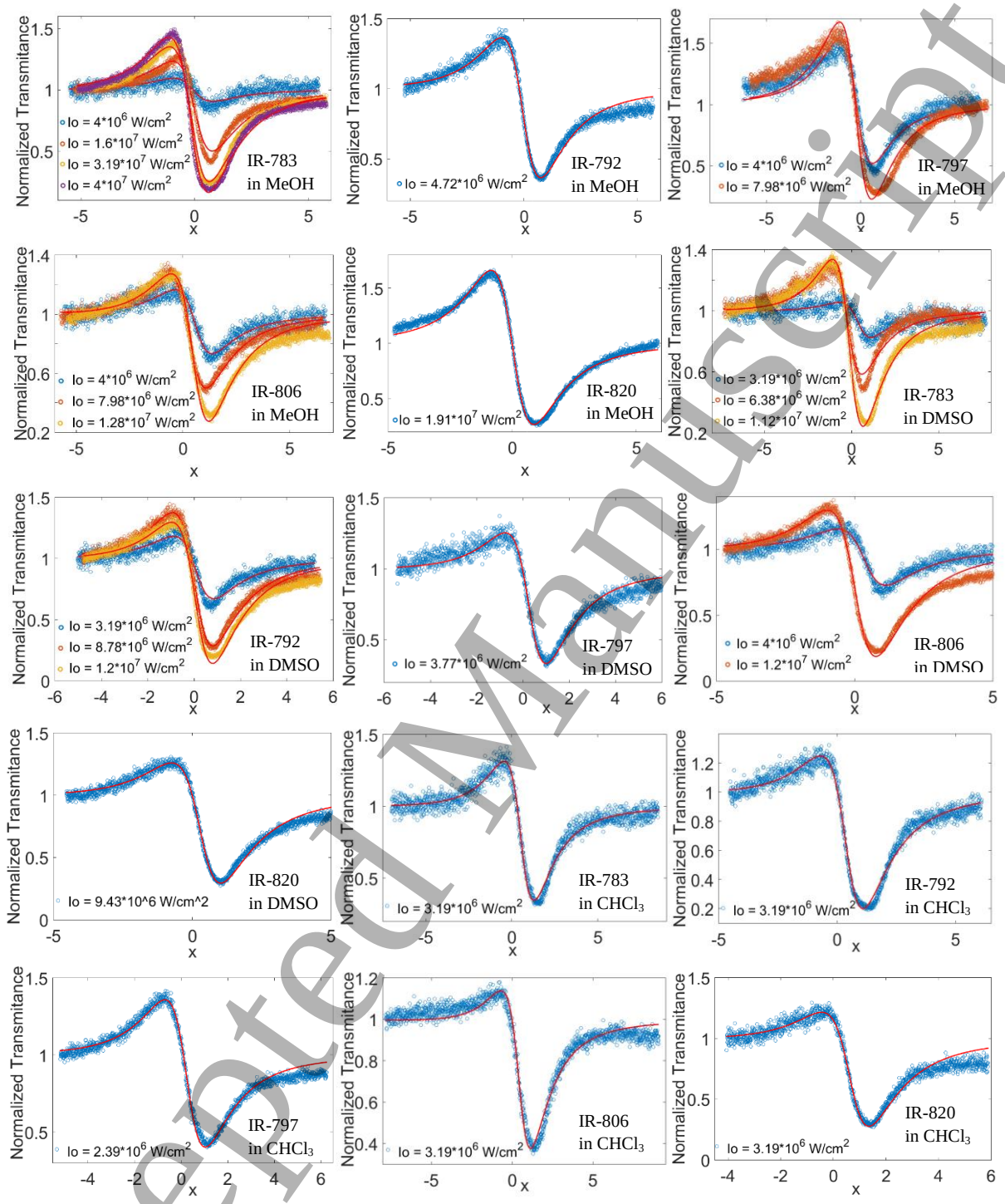

Figure 3 (b). Close Aperture traces of the heptamethine dyes showing nonlinear refractivity at mentioned intensities and solvents in the respective insets. The experimental data points are shown in colored circles, and the corresponding theoretical fit is shown in solid red lines.

Table 1. Nonlinear coefficients γ & β, Intensity at the focus (I_0), Ground state (σ_g) & Excited state (σ_{exc}) absorption cross sections as evaluated from theoretical fits of figure 3

			IR-783		
			MeOH		
Avg. Power (mW)	**I_0 (W/m^2)**	**γ (m^2/W)**	**β (m/W)**	**σ_g (m^2)**	**σ_{exc} (m^2)**
5-50	3.9×10^{10} - 3.9×10^{11}	- (1.2×10^{-15} – 9.9×10^{-16})	1.8×10^{-9} – 3.0×10^{-9}	2.94×10^{-23}	(1.04-1.4) $\times10^{-22}$
			DMSO		
4-20	3.2×10^{10} – 1.6×10^{11}	-(1.6-2.6) $\times10^{-15}$	3.0×10^{-8}	2.0×10^{-22}	(2.8-5.1) $\times10^{-21}$
			$CHCl_3$		
4	3.2×10^{10}	-6.3×10^{-15}	3.0×10^{-8}	3.7×10^{-23}	2.8×10^{-21}
			IR-792		
			MeOH		
Avg. Power (mW)	**I_0 (W/m^2)**	**γ (m^2/W)**	**β (m/W)**	**σ_g (m^2)**	**σ_{exc} (m^2)**
5-50	3.9×10^{10} - 3.9×10^{11}	- (1.2×10^{-15} – 9.9×10^{-16})	1.8×10^{-9} – 3.0×10^{-9}	2.94×10^{-23}	(1.04-1.4) $\times10^{-22}$
			DMSO		
4-20	3.2×10^{10} – 1.6×10^{11}	- (1.6-2.6) $\times10^{-15}$	3.0×10^{-8}	2.0×10^{-22}	(2.8-5.1) $\times10^{-21}$
			$CHCl_3$		
4	3.2×10^{10}	- 6.3×10^{-15}	3.0×10^{-8}	3.7×10^{-23}	2.8×10^{-21}
			IR-797		
			MeOH		
Avg. Power (mW)	**I_0 (W/m^2)**	**γ (m^2/W)**	**β (m/W)**	**σ_g (m^2)**	**σ_{exc} (m^2)**
5-10	(4.7-9.4) $\times10^{10}$	- (6.1-9.0) $\times10^{-15}$	1.9×10^{-9} – 1.0×10^{-8}	2.3×10^{-23}	(2.3-7.1) $\times10^{-23}$
			DMSO		
4-10	(3.7-9.4) $\times10^{10}$	- (1.0-4.8) $\times10^{-15}$	(7.6-8.5)$\times10^{-9}$	4.1×10^{-23}	(4.5-4.9) $\times10^{-23}$
			$CHCl_3$		
4	3.2×10^{10}	- 5.3×10^{-15}	1.52×10^{-8}	1.0×10^{-22}	2.8×10^{-22}
			IR-806		
			MeOH		
Avg. Power (mW)	**I_0 (W/m^2)**	**γ (m^2/W)**	**β (m/W)**	**σ_g (m^2)**	**σ_{exc} (m^2)**
5-16	3.9×10^{10}- 1.3×10^{10}	- (1.9-2.8) $\times10^{-15}$	(2.9-3.1) $\times10^{-9}$	6.3×10^{-23}	(6.4-6.6) $\times10^{-23}$
			DMSO		
5-15	(3.7-9.4)$\times10^{10}$	- 3.2 $\times10^{-15}$	(3.5-5.6)$\times10^{-9}$	6.8×10^{-23}	(7.1-9.9) $\times10^{-23}$
			$CHCl_3$		
4	3.2×10^{10}	- 5.4×10^{-15}	1.5×10^{-8}	1.0×10^{-22}	2.7×10^{-22}

IR-820					
MeOH					
Avg. Power (mW)	**I_0 (W/m^2)**	**γ (m^2/W)**	**β (m/W)**	**σ_g (m^2)**	**σ_{exc} (m^2)**
20	1.9×10^{11}	-1.5×10^{-15}	2.3×10^{-9}	1.0×10^{-22}	1.5×10^{-22}
DMSO					
10-30	9.4×10^{10} – 2.9×10^{11}	$-(2.9\times10^{-15}$ - $1.8\times10^{-16})$	$(1.3\text{-}3.4)\times10^{-9}$	4.2×10^{-23}	$(5.7\text{-}5.9)\times10^{-23}$
$CHCl_3$					
4	3.2×10^{10}	-9.6×10^{-15}	2.7×10^{-8}	1.8×10^{-23}	2.2×10^{-22}

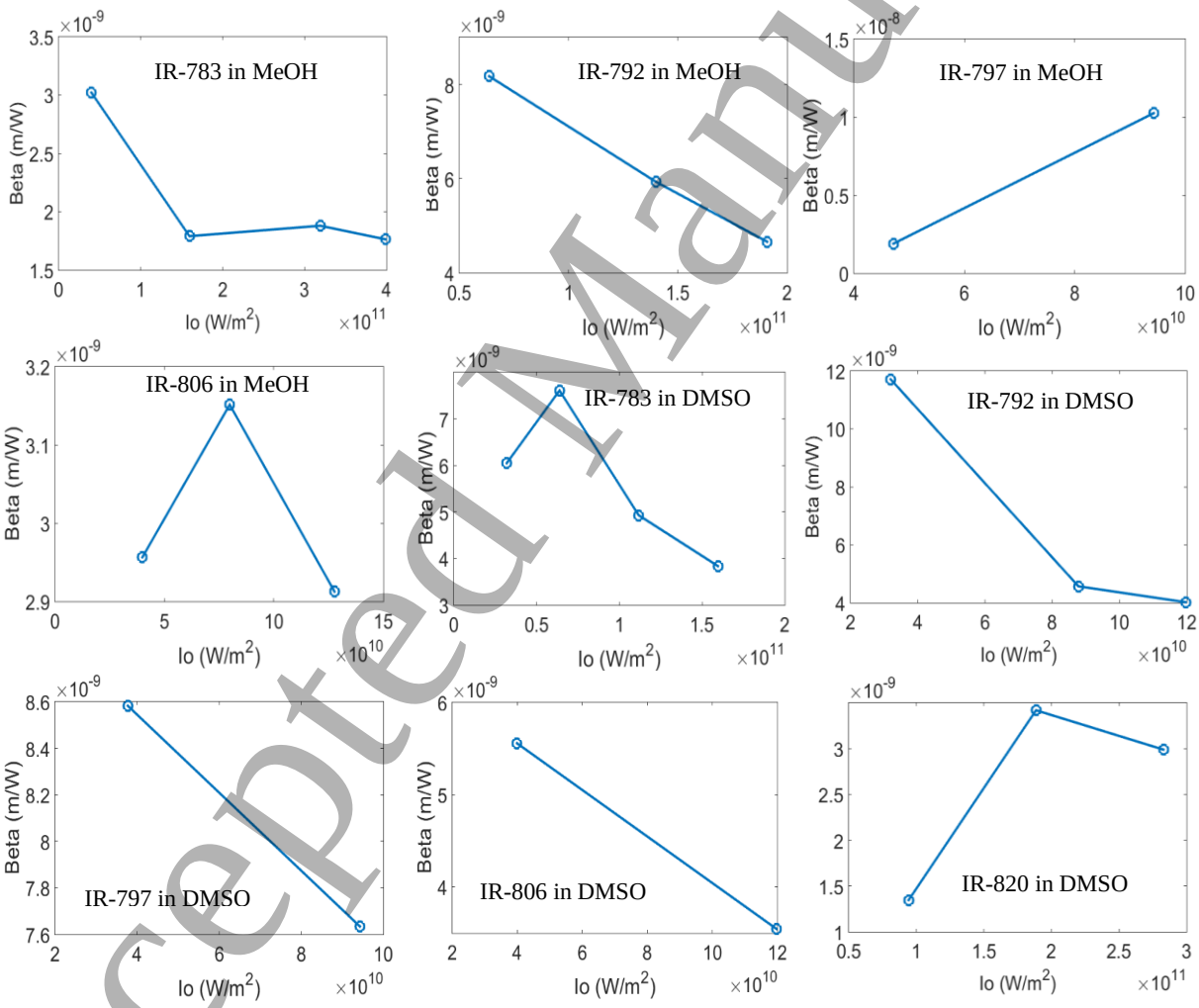

Figure 4. β (beta) versus I_0 plot to support the ESA assisted RSA except in five cases where power dependent Open aperture study (at various I_0) was not performed since no open aperture trace was obtained.

The excited state absorption in the visible region is further supported and observed under femtosecond excitations. For investigating ESA in these cyanines, femtosecond visible pump and supercontinuum

probe were employed in transient absorption studies. Excitation at 400 nm enabled us to observe ESA to higher excited singlet states. Subsequent probing at visible regions confirmed ESA leading to the observation of positive ΔOD in the spectrum. This positive ΔOD band was observed over the entire visible region with a rise time of some tens of picosecond (ps) and decay persisting till hundreds of ps to few nanoseconds. Dynamics at wavelengths corresponding to the band maxima were evaluated with a sum of multi-exponential functions convolved with the instrument response function (IRF).

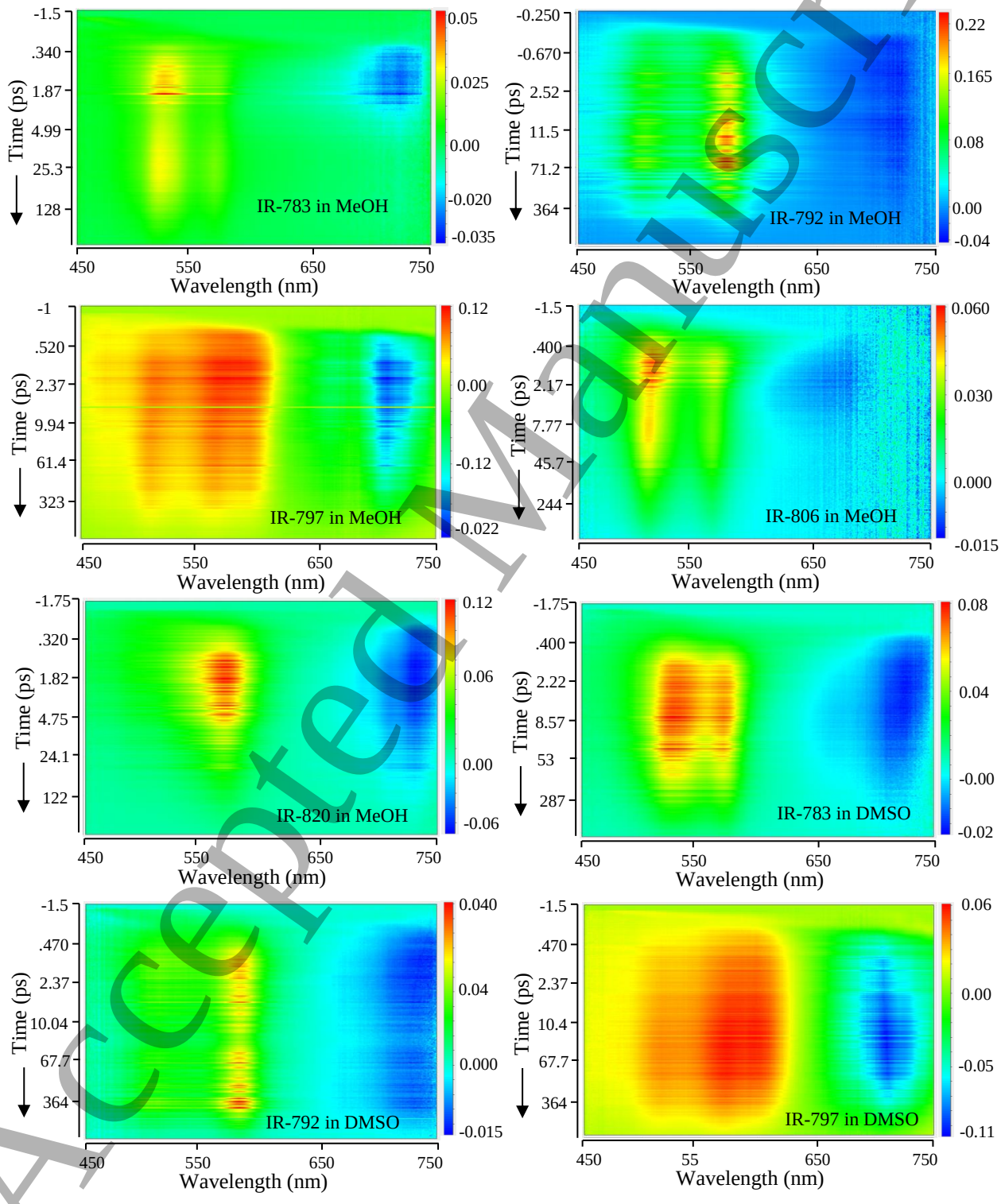

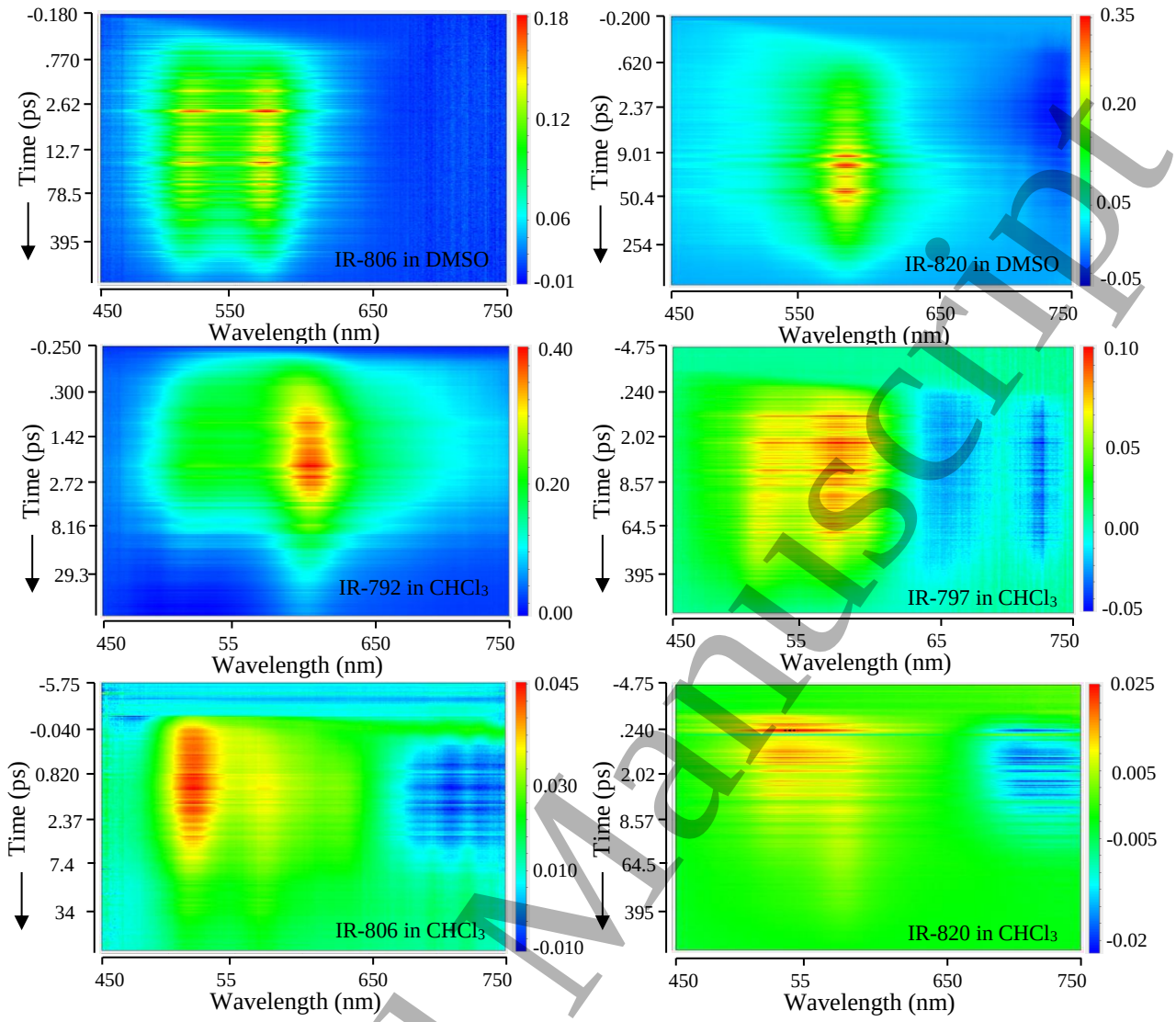

Figure 5. Spectrally dispersed intensity map of the transient Absorption Signal with 400 nm excitation and supercontinuum probe.

Time-resolved analysis of the transient spectra was performed utilizing Glotaran [47,48] software. The 2D contour plots conclusively show a considerable amount of absorption (positive ΔOD) in the 400-600 nm visible region. Since the molecules do not possess any linear ground state absorption in these regions, therefore these are essentially ESA signals characterized by a hot contour color. Starting from 650 nm, in all the cases, there exist cold spots, i.e., bleaching signals (negative ΔOD) which are the ground state absorption signals since molecules have significant absorptions in these regions. The analysis of time and wavelength-resolved (two-dimensional) datasets were performed by Global analysis and singular value decomposition (SVD) assuming that the observed data consist of the additive contributions of several components (chemical species), where each of the components has a characteristic spectrum and time-resolved concentration profile. Kinetic modeling was used to extract the excited state relaxation dynamics by fitting multi-exponential decays to the transients at selected wavelengths.

While utilizing the sequential model to visualize the spectral evolution of the spectra, corresponding EAS (evolution assisted spectra) were generated that finally resulted in the desired decay-associated spectra (DAS). Observation of ESA in the visible region of the transient absorption experiment also verifies the mechanism of ESA assisted RSA in these molecules. In the visible region, from 450 to 650 nm, we have observed positive ΔOD, i.e., absorption band as a result of excitation to higher singlet states. Correspondingly, when nanosecond pulses were used, we still found ESA assisted RSA, but in this case, excitation to the higher triplet states resulted from the first excited triplet (T_1). This observation is because the nanosecond pulse width is too long compared to the intersystem crossing rate and therefore, the population gets transferred from $S_1 \rightarrow T_1$. The excited state absorption bands in some of the molecules are shown in Figure-6 as extracted from Figure-5.

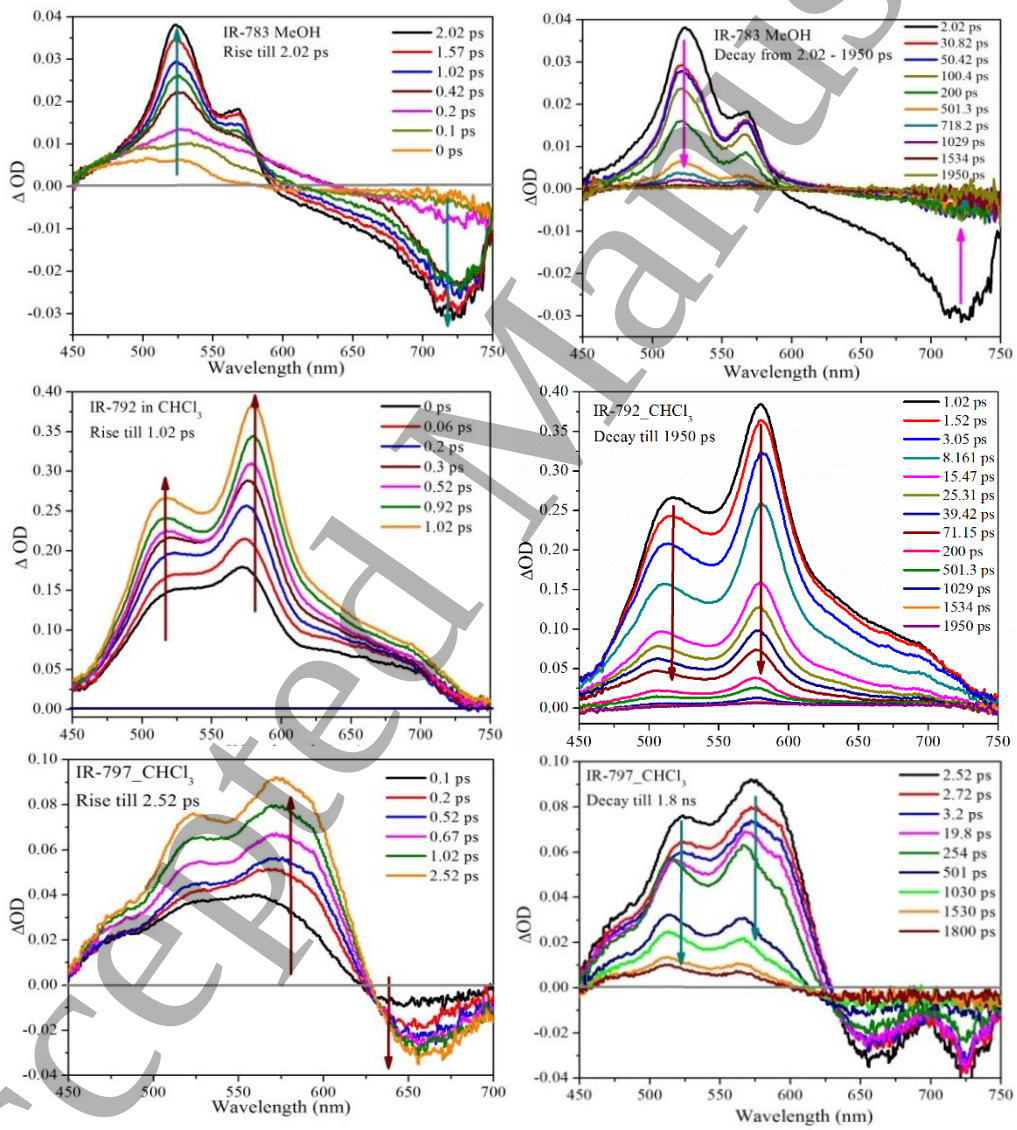

Figure 6. Femtosecond transient spectrum exhibiting ESA at visible excitations and supercontinuum probing.

Excited state relaxation dynamics were obtained by fitting the kinetic traces at selected wavelengths within the ESA band. Multiexponential decay parameters were needed to fit the traces, and a few of the plots are depicted in figure 7.

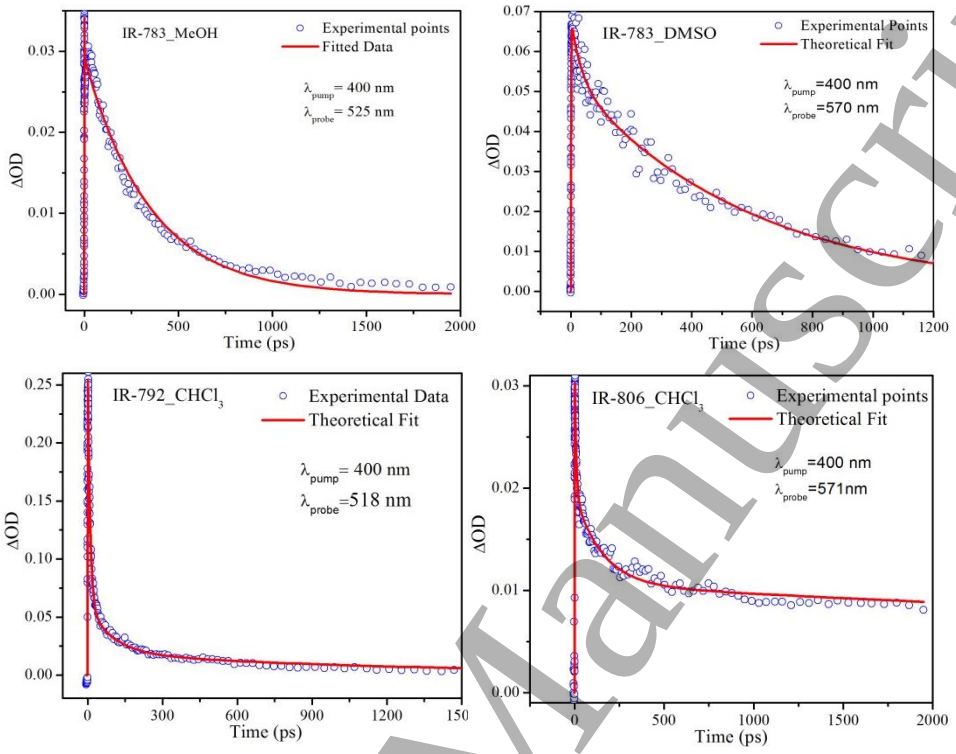

Figure 7. Kinetic traces of the excited state transients in some of the heptamethine dyes

The decay constants in case of IR-783 in MeOH consist of two-time constants as 2.35±0.4 ps (τ_1) and 348.1±0.7 ps (τ_2) respectively. τ_1 is essentially the solvation dynamics, and τ_2 corresponds to ground state recovery. For IR-792 in MeOH, τ_1 is 1.86±0.3 ps and τ_2 is 1.2±0.1 ns, indicating that the population does not relax to the ground state within the time-window of 2 ns. For IR-797 in MeOH, three distinct time-components are required, a fast component τ_1 of 825±200 fs that can be assigned to the rapid population re-equilibration process in the vibrational manifolds, which is justified from the fact that the vibrational sideband is dominating as shown in the absorption spectra and is growing almost as a separate band. The τ_2= 1.82±0.2 ps is correlated to solvation dynamics, and τ_3 is the ground state bleach recovery, that is 455.2±10 ps. In case of IR-806 in MeOH, τ_1=3.16±0.3 ps is intramolecular vibrational energy redistribution (IVR), τ_2=161.3±10 ps can be associated to population relaxation from higher excited singlet to first excited singlet which is pronounced in cases where absorption maxima are red to the excitation pulse spectra and finally the long-time decay of τ_3 = 1.6±0.3 ns. For IR-820 in MeOH, τ_1=4.37±0.5 ps, τ_2=40.9± 0.8 ps, and τ_3=252.7±5 ps. This molecule relaxes faster to ground state than other molecules.

Similarly, in DMSO solvent, IR-783 has decay constants τ_1=1.34±0.4 ps, τ_2=19.11±0.9 ps, and τ_3=557.2±12 ps respectively. IR-792 has time constants τ_1=1.86±0.3 ps and τ_2=1.8± 0.3 ns. Similarly,

IR-797 has a time constant ranging as τ_1=2.55±0.4 ps and τ_2=859.6± 5 ps. In IR-806 τ_1=5.58±0.6 ps, τ_2=123.2± 10 ps and τ_3=1.1±0.7 ns. Finally in IR-820, τ_1=6.11±0.5 ps, and τ_2=324.4± 10 ps, respectively.

Lastly, in $CHCl_3$, the decay components of IR-792 is τ_1=9.55±0.6 ps, τ_2=98.5± 6 ps, and τ_3=1.27±0.2 ns respectively. IR-797 has time components τ_1=14.33±0.8 ps, τ_2=358.4±10 ps, and τ_3=1.01±0.4 ns respectively. In IR-806 the kinetic decay parameters are τ_1=8.73±0.6 ps, τ_2=155.6±5 ps, and τ_3=11.1±0.5 ns respectively, though τ_3 value cannot be relied on and only reports the best-fitted parameters and has no physical interpretation. Finally, for IR-820 in $CHCl_3$, the decay components are τ_1=5.49 ±0.2 ps, τ_2=15.74± 5 ps, and τ_3=623.9±0.5 ns respectively.

From the contour plots and the time constants from fitted kinetics, it is very much clear that among all the solvents studied the five cyanines exhibits either biexponential or triexponential decays. The decay kinetics for each dye doesn't follow a mono-exponential decay confirming that the excited-state depopulation and restoration of the ground state population display different lifetimes. This also indicates that the dyes display nonlinear absorption in the visible region where there are contributions from additional states other than singlet excited as characterized by their excited states lifetimes. This effect is much more pronounced in case of $CHCl_3$ solvent which also signifies the increased photo-instability of the molecules in this solvent. The long lifetimes (τ_3) of the order of ~10ns in $CHCl_3$ (IR-806 & IR-820) and of the order of ~1-2 ns in $CHCl_3$ (for IR 792 & IR-797) confirms this behavior which is absent in another solvent. Thus, there is no evidence of the involvement of the additional intermediate states in MeOH and DMSO solvents that displays much faster time components with a biexponential decay and the absence of a τ_3.

4. Conclusion

We have experimentally investigated nonlinear absorption and refraction in a series of near-IR absorbing heptamethine cyanine dyes at non-resonant excitations in the visible region where these molecules have no or negligible linear ground state absorptions. We have shown that the studied heptamethine dyes are photo-stable in MeOH and DMSO solvents compared to $CHCl_3$ where these are photo-unstable under prolonged illuminations with low average powers far below their photo-dissociation limit. We found that all the five molecules under study exhibited strong excited-state absorption in the visible region, which corresponds to reverse saturable absorption. The phenomenon of ESA leading to RSA is a nonlinear process and is strongly governed by the laser pulse width and intensity. The ESA was observed in the 400 to 650 nm wavelength region resulting in the observation of a dip in the open aperture transmittance versus position plot in a Z-scan experiment at 527 nm. Nonlinear refractive coefficients were also extracted using close aperture studies, and we found that these molecules can act as potential nonlinear absorbers possessing nonlinear refraction for future use in the visible region. The response of these molecules under femtosecond illuminations was found to

be in ultrafast time scales and also supports the ESA mechanism operating in the visible region again indicating that indeed these molecules are fast nonlinear absorbers.

Acknowledgments

K. Makhal thanks UGC Govt. of India for a graduate fellowship. S. Maurya Thanks MHRD, Govt. of India for fellowship. D. Goswami thanks DST, MHRD Govt. of India for financial support and facilities. We all thank IIT Kanpur for facilities.

References

1. Tyutyulkov N, Fabian J, Mehlhorn A, Dietz F, Tadjer A 1991 Polymethine Dyes: Structure and Properties; St. Kliment Ohridski University Press: Sofia, Bulgaria

2. Jamie Lorett Gragg, Thesis "Synthesis of Near-Infrared Heptamethine Cyanine Dyes (2010) Georgia State University

3. Özhalici-Ünal H, Pow C L, Marks S A, Jesper L D, Silva G L, Shank N I, Jones E W, Burnette J M, Berget P B, Armitage B A 2008 *J. Am. Chem. Soc.* **130** 12620−21

4. Luby-Phelps K, Mujumdar S, Mujumdar R B, Ernst L A, Galbraith W, Waggoner A S 1993 *Biophys. J.* **65** 236−42

5. Wainwright M, Kristiansen J E 2003 Quinoline and cyanine dyes—putative anti-MRSA drugs *Int. J. Antimicrob. Agents* **22** 479−86

6. Luo S, Zhang E, Su Y, Cheng T, Shi C 2011 A review of NIR dyes in cancer targeting and imaging *Biomaterials* **32** 7127−38

7. Zhan W -h, Wu W –j, Hua J -l, Jing Y –h, Meng F -s, Tian H 2007 Photovoltaic properties of new cyanine–naphthalimide dyads synthesized by 'Click' chemistry *Tetrahedron Lett.* **48** 2461−5.

8. Castro F A, Faes A, Geiger T, Graeff C F O, Nagel M, Nüesch F, Hany R 2006 On the use of cyanine dyes as low-bandgap materials in bulk heterojunction photovoltaic devices *Synth. Met*. **156** 973−8

9. Sun R, Yan B –L, Ge J –F, Xu Q –f, Li N –J, Wu X –Z, Song Y –L, Lu J -M 2013 Third-order nonlinear optical properties of unsymmetric pentamethine cyanine dyes possessing benzoxazolyl and benzothiazolyl groups *Dyes Pigm.* **96** 189−95

10. Zheng Q, He G S, Prasad P N 2009 A novel near IR two-photon absorbing chromophore: Optical limiting and stabilization performances at an optical communication wavelength *Chem. Phys. Lett.* **475** 250−55

11. Bazylinska U, Pietkiewicz J, Saczko J, Nattich-Rak M, Rossowska J, Garbiec A, Wilk K A 2012 Nanoemulsion-templated multilayer nanocapsules for cyanine-type photosensitizer delivery to human breast carcinoma cells *Eur. J. Pharm. Sci.* **47** 406-20

12. Bouit P.-A, Aronica C, Toupet L C, Le Guennic B, Andraud C, Maury O 2010 Continuous Symmetry Breaking Induced by Ion Pairing Effect in Heptamethine Cyanine Dyes: Beyond the Cyanine Limit *J. Am. Chem. Soc.* **132** 4328−35

13. Fabian J, Hartmann H 1980 Light Absorption of Organic Colorants: Theoretical Treatment and Empirical Rules, AAA ed. Springer-Verlag, New York

14. Guarin C A, P Juan, Monsalve V, Arteaga R L-, Peon J 2013 Dynamics of the Higher Lying Excited States of Cyanine Dyes. An Ultrafast Fluorescence Study *J. Phys. Chem. B* ***117*** 7352–62

15. Pisoni D S, Todeschini L, Borges A C A, Petzhold C L, Rodembusch F S, Campo L F 2014 Symmetrical and Asymmetrical Cyanine Dyes. Synthesis, Spectral Properties, and BSA Association Study *J. Org. Chem.* **79** 5511–20

16. Kasha M 1950 *Discuss. Faraday Soc.* **9** 14−19

17. Bouit P.-A, Spaenig F, Kuzmanich G, Krokos E, Oelsner C, Garcia-Garibay M A, J L Delgado, Martin N, Guldi D M 2010 Efficient Utilization of Higher-Lying Excited States to Trigger Charge-Transfer Events *Chem. Eur. J.* **16** 9638−45

18. Kasatani, K, Sato H 1996 Viscosity-Dependent Decay Dynamics of the S2 State of Cyanine Dyes with 3, 5, and 7 Methine Units by Picosecond Fluorescence Lifetime Measurements *Bull. Chem. Soc. Jpn.* **69** 3455−60

19. Rehak V, Novak A, Titz M 1977 $S_2 \rightarrow S_0$ Fluorescence of cryptocyanine solutions *Chem. Phys. Lett.* **52** 39−42

20. Oulianov D A, Dvornikov A S, Rentzepis P M 2002 Optical limiting and picosecond relaxation of carbocyanines upper electronic states *Opt. Commun.* **205** 427−36

21. Streitwieser A 1963 Molecular Orbital Theory, Wiley, New York, London

22. Bayliss, N S 1949 Conjugated Compounds. II. Simple Potential Energy Functions, Absorption Spectra, and Ionization in Linear Polyenes *Australian Journal of Scientific Research, Series A: Physical Sciences,* **3** 109-127

23. Kuhn H 1949 A quantum mechanical theory of light absorption of organic dyes and similar compounds J. *Chem. Phys*. **17** 1198-1212

24. Simpson W T 1951 A Mathematical Treatment of the Color of the Merocyanine Dyes *J. Am. Chem. Soc.* **73** 5359-63

25. Konig W 1926 Conception of the "polymethine dyes" and a general dye formula derived therefrom as the basis of a new system of dye chemistry *J. Prakt. Chem.* **112** 1-36

26. Radeglia R, Dähne S, Hartmann H 1965 RinggroBeneinfluB cyclischer Aminogruppen auf dien-Elektronenverteilung einfacher Cyanine *J. Prakt. Chemie* **312** 1081–86

27. Dahne S, Leupold D 1966 Coupling Principles in Organic Dyes *Angew. Chem.* Int. Ed. **5** 984-93

28. Dahne S 1978 Color and constitution: one hundred years of research *Science* **199** 1163-7

29. Dahne S, Radeglia R 1971 Revision der Lewis-Calvin-Regel zur charakterisierung vinyloger. Polyen- und polymethinähnlicher verbindungen *Tetrahedron* **27** 3673–3693.

30. Lepkowicz R S, Przhonska O V, Hales J M, Fu J, Hagan D J, van Stryland E W, Bondar M V, Slominsky Y L, Kachkovski A D 2004 Nature of the electronic transitions in thiacarbocyanines with a long polymethine chain *Chem. Phys.* **305** 259–70

31. Ishchenko A A 1991 Structure and spectral-luminescent properties of polymethine dyes *Russian Chem. Rev*. **60** 865-84

32. Gaikwad P 2009 On the optical limiting and Z-scan of hexamethylin-dotricarbocyanine perchlorate dye *Opt. Mater*. **31** 1559−63

33. Bouit P -A, Wetzel G, Berginc G, Loiseaux B, Toupet L, Feneyrou P, Bretonniere Y, Kamada K, Maury O, Andraud C 2007 Near IR Nonlinear absorbing chromophores with optical limiting properties at telecommunication wavelengths *Chem. Mater*. **19** 5325 −35

34. Hales J M, Zheng S, Barlow S, Marder S R, Perry J W 2006 Bisdioxaborine polymethines with large third-order nonlinearities for all-optical signal processing *J. Am. Chem. Soc.* **128** 11362-3

35. Bellier Q, Makarov N S, Bouit P -A, Rigaut S, Kamada K, Feneyrou P, Berginc G, Maury O, Perry J W, Andraud C 2012 Excited state absorption: a key phenomenon for the improvement of biphotonic based optical limiting at telecommunication wavelengths *Phys. Chem. Chem. Phys.* **14** 15299–307

36. Padilha L A, Webster S, H Honghua, Przhonska O V, Hagan D J, Van Stryland E W, Bondar M V, Davydenko I G, Slominsky Y L, Kachkovski A D 2008 Excited state absorption and decay kinetics of near IR polymethine dyes *Chem. Phys.* **352** 97–105

37. Li Z, Zhao P, Tofighi S, Sharma R, Ensley T R, Jang S-H, Hagan D J, Van Stryland E W, Jen A K -Y 2016 Zwitterionic cyanine–cyanine salt: structure and optical properties *J. Phys. Chem. C* **120** 15378−84

38. Li Z, Kim H, Chi S-H, Hales J M, Jang S-H, Perry J W, Jen A K-Y 2016 Effects of counterions with multiple charges on the linear and nonlinear optical properties of polymethine Salts *Chem. Mater.* **28** 3115−21

39. M. Sheik-Bahae, A. A. Said, T.–H. Wei, D. J. Hagan and E. W. V. Stryland 1990 Sensitive measurement of optical nonlinearities using a single beam *IEEE J. Quantum Electron*. **26** 760-9

40. He G S, Yuan L, Cheng N, Bhawalkar J D, Prasad P N 1997 Nonlinear optical properties of a new chromophore *J. Opt. Soc. Am. B* **14** 1079-87

41. He G S, Yuan L, Weder C, Smith P, Prasad P N 1998 Optical power limiting and stabilization based on a novel polymer compound *IEEE J. Quantum Electron.* **34** 2279-85

42. Henari F Z, Blau W J, Milgrom L R, Yahioglu G, Philips D, Lacey J A 1997 *Chem. Phys. Lett.* **267**, 229-33

43. Henari F Z 2001 *J. Opt. A: Pure Appl. Opt.* **3** 188-90

44. Chapple P B, Staromlynska J, Hermann J A, Mckay T J, Mcduff R G 1997 *J. Nonlinear Opt. Phys. Mater.* **6** 251-93

45. Lin M, Li H P, Tang S H, Ji W 2000 Determination of nonlinear absorption and refraction by single Z-scan method *Appl. Phys. B: Lasers Opt.* **70** 587–91

46. Liu X, Guo S, Wang H, Hou L 2001 Theoretical study on the closed-aperture Z-scan curves in the materials with nonlinear refraction and strong nonlinear absorption *Opt. Commun.* **197** 431–37

47. Snellenburg J J, Laptenok S, Seger R, Mullen KM, van Stokkum IHM 2012 Glotaran: A Java-Based Graphical User Interface for the R Package TIMP *J. Stat. Soft.* **49** 1-22

48. Mullen K M, van Stokkum I H M 2007 TIMP: An R package for modeling multi-way spectroscopic measurements *J. Stat. Soft.* **18** (3) 1-46